

Numerical model of rf glow discharges

J.-P. Boeuf

*Centre de Physique Atomique de Toulouse, Université Paul Sabatier,
118, route de Narbonne, 31062 Toulouse Cédex, France*

(Received 24 February 1987)

Theoretical predictions are given of the spatiotemporal distribution of charged-particle densities and electric field in a radio-frequency glow discharge. The model is based on a numerical solution of the continuity equations for electrons, positive ions, and negative ions coupled with Poisson's equation. The influence of frequency and gas composition (electropositive versus electronegative gas) on the discharge properties is analyzed and compared (qualitatively) with experimental results. In the case of electronegative gas mixtures, and at low frequencies (of the order and less than the ion plasma frequency), the numerical model predicts the formation of double layers at the plasma-sheath boundaries, in agreement with recent experimental measurements based on spectroscopic plasma-diagnostic techniques.

I. INTRODUCTION

The ability of glow discharges to provide high-temperature chemistry at low gas temperatures has made it very attractive for plasma chemistry. For this reason, rf glow discharges are widely used in the microelectronics industry, for the deposition and etching of thin solid films. The understanding of charged-particle transport in the sheaths is of paramount importance for a better control and optimization of industrial reactors. In spite of the widespread use of rf discharges in microelectronic manufacturing, our understanding of the physical and chemical mechanisms of the discharge is still incomplete.

On the other hand, due to the recent development of very efficient plasma diagnostic techniques¹⁻⁶ such as LIF (laser-induced fluorescence) and LOG (laser optogalvanic) it is now possible to obtain complete space-time mappings of the electric field⁶ in the discharge, and it seems very useful to develop self-consistent numerical models in connection with the experimental approach.

A complete model of rf discharges used in plasma chemical reactors must account for the coupled interactions between charged-particle kinetics, neutral-particle kinetics and chemistry, and electric field; this is indeed a very formidable task and no complete self-consistent model has yet been developed. However, valuable information can be obtained from simplified models where only one aspect of the discharge is analyzed, some assumptions being made on the others: Kushner⁷ obtained the time-averaged spatially dependent electron energy distribution functions and excitation rates in rf discharges in CO and CF₄, assuming a given form of the electric field in the sheaths. Emphasis was placed on the plasma chemistry in the numerical models developed by Kushner⁸ and Chatham and Gallagher.⁹ Graves and Jensen¹⁰ presented a self-consistent numerical model accounting for the coupling between charged-particle transport and electric field in a model electropositive gas (see also Refs. 11 and 12 where similar numerical models are presented for rf discharges in argon).

In this paper, as in Refs. 10-12, we focus on the physical aspect of the discharge, and no attempt is made to treat self-consistently the plasma chemistry involved in a practical situation. The purpose of this paper is to study some general features of rf discharges, and to analyze the influence of some parameters such as frequency and gas composition (electronegative versus electropositive gas) on the discharge regime: It has been shown by Gottscho and Gaebe⁶ that the presence of negative ions in rf discharges, at frequencies of the order or less than the ion plasma frequency, can induce some specific effects on the charge and field distributions. These effects are analyzed in the present paper, with a self-consistent electrical model of the discharge.

The model is based on a self-consistent solution of the electron and ion continuity and momentum transfer equations coupled with Poisson's equation for a given potential waveform between electrodes, and assuming local equilibrium between charged particle kinetics and electric field.

The equilibrium hypothesis is a closure relation which enables us to describe the electron and ion kinetics with the continuity and momentum transfer equations instead of the full Boltzmann equation. Although numerical methods for solving the Boltzmann equation for a given field distribution are now available^{7,13-15} the coupling between the Boltzmann equation and Poisson's equation in dc or rf glow discharges is still a difficult numerical problem and no satisfactory solution has yet been obtained (some attempts have been made to solve the Boltzmann transport equation for electrons assuming only forward and backward scattering, coupled with the ion continuity equation and Poisson's equation in a dc glow discharge¹⁶⁻¹⁸).

In the local equilibrium approximation which has been used in a number of analytical or numerical models of dc glow discharges,¹⁹⁻²² transport coefficients (drift velocity, diffusion coefficients, ionization, and attachment coefficients) are assumed to depend only on the local electric field (they are actually functionals of the local velocity distribution function which is unknown); the validity of

this assumption is discussed in Sec. II B.

Let us note that attempts to improve the macroscopic description of the electron kinetics in dc or transient glow discharges have been made by Ingold,²³ Boeuf *et al.*,²⁴ Bayle *et al.*,²⁵ Graves and Jensen,¹⁰ and Richards *et al.*¹² In Refs. 10, 12, 23, and 25 the electron energy equation was added to the continuity and momentum transfer equations with different closure relations (a given shape of the electron distribution function was assumed in Ref. 23, while some assumptions concerning the source terms of the moment equations are made in Refs. 10, 12, and 25); Boeuf *et al.*²⁴ used the concept of effective field suggested by Schofield²⁶ and developed by Segur *et al.*¹⁴ In this approach (see also Ref. 27) the local ionization coefficient is assumed to depend not only on the local field but on an effective field which accounts for the large field variations in the cathode fall region (a semiempirical relation between effective field and real field distribution in the gap is obtained from comparisons with solutions to the Boltzmann transport equation).

In spite of the roughness of the local equilibrium assumption, the model presented in this paper can provide, in a limited range of frequency, power and gap length (see Sec. II B), a correct description of the main features of rf discharges (Sec. III).

The theoretical background of the model is presented in Sec. II, including the basic equations, boundary conditions and data in Sec. II A, an estimation of the range of validity of the model in Sec. II B, and the numerical techniques in Sec. II C. The results are presented and discussed in Sec. III: the space and time variations of charge-particle densities and electric field in an electropositive gas are shown in Sec. III A, while the effect of negative ions on the discharge properties is analyzed in Sec. III B. Section IV contains the general conclusions of this work. Additional details concerning the numerical techniques are given in the Appendix.

II. THEORY

A. Basic equations and data

As mentioned above, electron and ion transport is described with the continuity and momentum-transfer equations in a one-dimensional, parallel-plate geometry with conducting electrodes; the following set of coupled nonlinear equations is therefore considered:

$$\partial_t n_e + \partial_x (n_e v_e) = n_e |v_e| (\alpha - \eta), \quad (1)$$

$$n_e v_e = n_e W_e - \partial_x (n_e D_e), \quad (2)$$

$$\partial_t n_p + \partial_x (n_p v_p) = \alpha n_e |v_e| - r n_n n_p, \quad (3)$$

$$n_p v_p = n_p W_p - \partial_x (n_p D_p), \quad (4)$$

$$\partial_t n_n + \partial_x (n_n v_n) = \eta n_e |v_e| - r n_n n_p, \quad (5)$$

$$n_n v_n = n_n W_n - \partial_x (n_n D_n), \quad (6)$$

$$dE/dx = |e|/\epsilon_0 (n_p - n_e - n_n), \quad E = -dV/dx, \quad (7)$$

$$\int_0^d -E(x,t) dx = V_g(t).$$

n_e , n_p , n_n are, respectively, the electron, positive-ion,

and negative-ion densities; W_k and D_k are the drift velocity and diffusion coefficient of particles of type k ; α and η are, respectively, the ionization and attachment coefficients; r is the positive-ion–negative-ion recombination rate; E and V are the local electric field and potential. All these parameters depend on position x and time t ; d is the gap length and V_g the potential between electrodes.

The boundary conditions used in the calculations are as follows.

The potential waveform between electrodes is given (the external circuit is not considered) and is assumed to be of the form

$$V_g(t) = V_{dc} + V_{rf} \cos(\omega t), \quad (8)$$

where $\omega = 2\pi F$ (F is the frequency).

The boundary conditions for the charged-particle flux on the electrodes are considered to be mixed:²⁸ the drift component ($n_k W_k$) of the particle flux ($n_k v_k$) is set to zero if the particle velocity is away from the electrode; the diffusion component ($-\partial_x n_k D_k$) of the particle flux is set to zero on the electrode surface at any time (zero density gradients). When secondary electron emission is considered the flux of electrons leaving the electrode is given by $\gamma |n_p W_p(s,t)|$ [γ is the secondary emission coefficient, $n_p W_p(s,t)$ is the positive-ion flux on the electrode surface; $s=0$ or d].

Results are presented in Sec. III for helium and for a model electronegative gas. In the case of helium, electron and positive-ion transport coefficients (drift velocity and ionization coefficient) are taken from Ward;²⁰ electron and ion diffusion coefficients are supposed to be constant (respectively, 10^6 and 0.5×10^3 cm²/s at $p=1$ torr); gas temperature is supposed to be constant and uniform in the gap.

In order to study the specific effects of attachment on the discharge properties the model electronegative gas has been defined as follows.

Electrons and positive ions have the same transport coefficients as in helium (drift velocity, diffusion coefficient, and ionization coefficient).

Negative ions have the same drift velocity (opposite sign) and diffusion coefficient as positive ions.

The attachment coefficient is supposed to decrease with increasing fields according to $\eta/p = A/(1 + BE/p)$ where $A=0.2$ cm⁻¹ torr⁻¹ and $B=1$ V⁻¹ cm torr.

Ion-ion recombination coefficient r is set to 10^{-6} cm³/s.

Although this electronegative model gas is unrealistic, it makes possible the analysis of the changes in the discharge properties which are induced only by the presence of negative ions (everything else being kept constant).

B. Validity of the model

The local equilibrium assumption implies that the transport coefficients (α , η , W_k , and D_k) depend on space and time (x,t) only through the local value of the electric field $E(x,t)$: The transport coefficients at position x and time t are assumed to be the same as those which could be measured or calculated under a uniform and constant electric field equal to $E(x,t)$ (hydrodynamic regime²⁹). In the hydrodynamic regime, the force term

and the collision term of the Boltzmann equation are much larger than the free fall terms. Deviations from the hydrodynamic regime appear near an electron source or sink (electrodes), or when the electric field exhibits large spatial or temporal variations.

Let us first consider the problem of time varying fields. The relaxation of the electron-velocity distribution function (EVDF) can be characterized by the energy and momentum dissipation frequencies^{30,31} (normalized with respect to the gas pressure):

$$\frac{\nu_e}{p} = \frac{2m}{M} \frac{\nu_{me}}{p} + \sum \frac{\nu_k}{p},$$

$$\frac{\nu_{mT}}{p} = \frac{\nu_{me}}{p} + \sum \frac{\nu_k}{p},$$

where ν_{me} is the elastic momentum transfer collision frequency and ν_k is the collision frequency for the k th inelastic process; m/M is the electron molecule mass ratio.

For field frequencies such that $\omega/p \ll \nu_{mT}/p$ (ν_{mT}/p is larger than $10^8 \text{ s}^{-1} \text{ torr}^{-1}$ for the conditions which are considered in the present work), a quasistationary description of the anisotropic part of the EVDF is correct [note also that the time derivative terms which should normally appear in the momentum transfer equations (2), (4), and (6) can be neglected only if the above condition is satisfied]. For frequencies such that $\omega/p \ll \nu_e/p$, the isotropic part of the EVDF follows the rf field in a quasistationary way, except when the field passes zero.^{30,31} In the conditions which are considered in the present work, the energy dissipation frequency of the high-energy part of the distribution function (beyond the first inelastic threshold) is larger than $10^7 \text{ s}^{-1} \text{ torr}^{-1}$. For frequencies less than $10^7 \text{ s}^{-1} \text{ torr}^{-1}$, it is therefore not unrealistic to assume that the ionization coefficient follows the time variations of the rf field in a stationary way. An estimate of the time scale for the relaxation of the electron energy distribution function can also be given by the energy exchange collision frequency defined by Frost and Phelps³² and leads to the same conclusion (see Refs. 33 and 34 where the validity of the local equilibrium assumption is discussed for rf plasmas in SF_6 and Cl_2 , respectively). Note also that the energy dissipation frequency may be much smaller at lower energy (where elastic collisions are dominant); the low-energy part of the distribution function is much less modulated than the high-energy part.^{30,31} For a given frequency, attachment (which occurs generally at low energy) will therefore be more affected by nonequilibrium effects induced by the time varying field than ionization.

Nonlocal effects can also be due to the spatial variations of the electric field.¹³⁻¹⁸ In a dc discharge, the electrons emitted by the cathode are accelerated in the sheath and lose their energy in the glow through inelastic collisions. The local equilibrium assumption overestimates ionization in the sheath (electrons are emitted by the cathode with a much lower energy than the equilibrium energy corresponding to the cathode field), and underestimates ionization in the glow (high-energy electrons entering the negative glow are not taken into account). This can lead to large errors for strongly abnormal glow discharges where

the almost collisionless sheath acts as an electron gun. However, for normal or moderately abnormal dc glow discharges, the global multiplication factor obtained with the local equilibrium assumption is close to the multiplication factor obtained by Monte Carlo techniques.¹⁵ Since the discharge parameters (discharge current, sheath thickness) depend more on the total multiplication factor than on the exact form of $\alpha(x)$, we conclude that the local equilibrium assumption can provide realistic results in a limited range of applied voltage. In the present work we restrict ourselves to rf voltages and maximum sheath lengths of the order of the dc voltages and sheath lengths corresponding to normal or moderately abnormal glow discharges in helium: $V_{\text{rf}} < 500 \text{ V}$, $pd_c > 1 \text{ torr cm}$ (d_c is the sheath thickness).

C. Numerical Techniques

Due to the high nonlinearity and strong coupling of Eqs. (1)–(7), the treatment of these equations is a difficult numerical problem. Ward²⁰ used a shooting technique to obtain the electric field distribution in the case of dc glow discharges (charged-particle diffusion was not considered in this model). This method, improved by Davies and Evans²² (see also Duke¹⁸), is, however, unable to deal with large total current densities. Non-self-sustained steady-state glow discharges have been studied by Lowke and Davies²¹ using two different numerical approaches: The first one was based on an explicit relaxation method where steady state is obtained from time-dependent equations (with distorted time steps in order to accelerate convergence); in the second approach the steady-state equations are solved using a predictor corrector method. Bayle *et al.*²⁵ analyzed only transient regimes due to the excessive amount of computation time needed to reach steady state. The problem of modeling rf discharge is even more complex in terms of numerical analysis, since it implies a two-dimensional (space and time) treatment. Graves and Jensen¹⁰ chose to solve the rf problem as a boundary value in time, using a Fourier series expansion to represent the time variations of the unknown functions and a nonuniform mesh in space. The resulting set of nonlinear equations was solved using the Newton-Raphson method. This matrix iterative technique is very demanding in terms of computing resources (memory and computation time) and cannot be used on most computers.

Considerable work concerning numerical methods for solving systems of non linear equations similar to (1)–(7) has been done in the field of semiconductor physics, for the modeling of one- and two-dimensional semiconductor devices (see, for example, the reviews by Selberherr,³⁵ Selberherr and Ringhofer,³⁶ and Snowden³⁷). The problem of electron and hole transport in semiconductors is parallel to the problem of charged-particle transport in weakly ionized gases and a systematic comparison of difficulties and progress in both fields would be very useful.

The implicit difference scheme used in the present work has been developed by Scharfetter and Gummel³⁸ for the modeling of a silicon Read diode oscillator and is currently used in a number of numerical models of semiconductor devices^{35,39,40} and fluid dynamics.⁴¹ The rf problem is

solved by following the time evolution of the discharge from a given set of initial conditions, until harmonic steady state is reached [$A(x, t + T) = A(x, t)$, A being one of the unknown functions, and $T = 1/F$]. The nonlinear system of equations is solved by a procedure based on alternate solutions of the Poisson and continuity equations. This method implies the time integration of the transient equations over a large number of cycles (a few tens to a few hundreds, depending on discharge conditions). Explicit time advancement numerical methods for continuity equations are subject to severe limitations on the integration time step (Courant-Friedrichs-Lewy and Von Neumann conditions²⁸) and are therefore not well suited to the rf problem. The main advantage of the implicit exponential scheme of Scharfetter and Gummel³⁸ is its robustness, stability, and ability to deal with situations where either the drift or the diffusion component of the current density is dominant (these situations correspond, respectively, to the sheath and plasma regions). The difference scheme of Scharfetter and Gummel has been adapted to the problem of charged-particle transport in gases and is briefly described in the Appendix.

The time integration step used in the calculations was always less than $2.5 \times 10^{-3} T$; convergence was assumed to be reached when the time-averaged (over one cycle) conduction current density on the electrodes changed by less than 0.01% over two consecutive cycles. The zero divergence of the total current density (conduction plus displacement) at any time of the cycle was also checked at steady state. The computation time was of the order of one to a few hours on a mini computer HP1000 A900.

III. RESULTS

Results are presented for helium and for a model electronegative gas (see Sec. II A) in the case of a purely rf potential waveform ($V_{dc} = 0$), and for frequencies between 50 kHz and 10 MHz (parallel plate conducting electrodes; secondary electron emission $\gamma = 0.1$; gas pressure $p = 1$ torr; gas temperature $T_g = 300$ K; gap length $d = 4$ cm). Most of the results given in this section (except Figure 14) have been obtained for $V_{rf} = 500$ V.

A. Helium

The spatial variations of the electric field, and electron and ion densities at four different times of a rf cycle are shown in Fig. 1 for $F = 10$ MHz (the field is positive when directed towards the left electrode). As can be expected for high frequencies, the ion density does not respond to the time-varying field and is only sensitive to the time-averaged field. The formation of positive net charge density in the sheaths is therefore entirely due to electron motion: Electrons are swept from the sheath into the plasma during the cathodic part of the cycle, whereas they flow to the electrode during the anodic part. The sheath expansion provides energy to the secondary electrons and to the "plasma electrons" (electrons flowing from the plasma to the electrode during the preceding sheath contraction, and which have not reached the electrode before the beginning of the sheath expansion); this property of rf discharges to impart energy to the plasma electrons makes

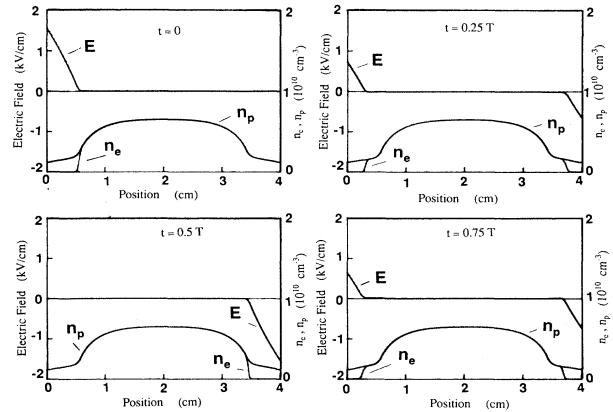


FIG. 1. Spatial variations of the electric field and charged-particle densities at four different times of a rf cycle (helium, $F = 10$ MHz, $V_{rf} = 500$ V).

them more efficient than dc discharges.

The electron density is modulated only in the sheath and is nearly constant in the plasma. The plasma density is around $5 \times 10^9 \text{ cm}^{-3}$. The electric field in the sheaths decreases almost linearly at any time of the cycle. The sheath expansion and contraction appear more clearly on Fig. 2 where the space-time variations of the electric field over one cycle are displayed. In agreement with experimental results⁴² and previous theoretical works,⁴³ the sheath expansion and collapse are nearly symmetrical at high frequencies. The cathodic part of the cycle lasts much longer than the anodic part due to the large disparity in electron and ion drift velocities: The time-averaged total conduction current to the electrodes (and in the gap)

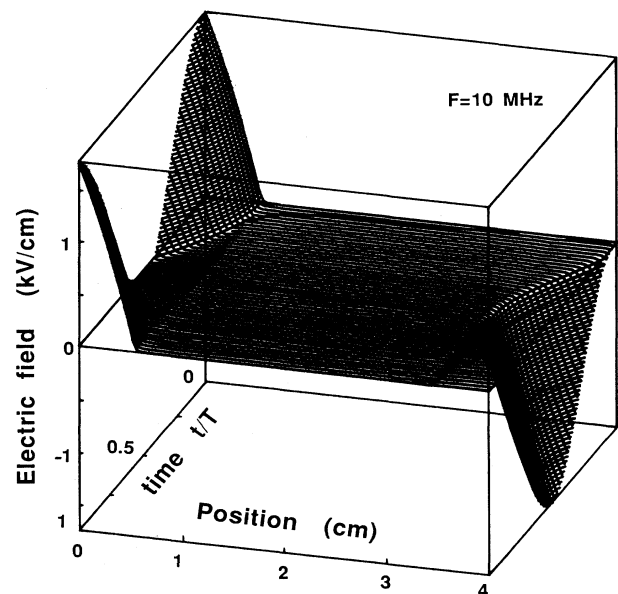


FIG. 2. Spatio-temporal variations of the electric field (same conditions as Fig. 1).

must be zero (purely rf voltage) as can be checked in Fig. 3 which shows the time variations of the electron, ion, displacement, and total current densities on the left electrode. It appears that the displacement current on the electrode is dominant and much larger than the ion current density during the cathodic part of the cycle ($0 < t < 0.35T$ and $0.55T < t < T$); during the anodic part of the cycle, the displacement current density decreases sharply and the electron current density becomes dominant. The total current density is phase-shifted from the applied voltage, but presents no significant distortion. As expected, the phase shift between current and voltage is close to $\pi/2$, the sheath being mainly capacitive at high frequencies.

The total current (displacement plus conduction) in the gap is spatially uniform at any time of the cycle; the electron contribution to the conduction current is dominant in the plasma since ions are much less sensitive to the time variations of the electric field. Figure 4 displays the space-time variations of the electron conduction current density in the gap over one rf cycle and shows that electron conduction is large and spatially constant in the plasma. The displacement current (Fig. 5) exhibits large time variations in the sheaths and is much smaller than the electron conduction current density in the plasma. The electron conduction current couples to the displacement current (Figs. 4 and 5) in the sheaths in agreement with the numerical results of Graves and Jensen.¹⁰

The sheath thickness does not change very much when the rf potential is decreased from 500 to 150 V, for $F=10$ MHz [see Fig. 14(a)]. When the frequency is decreased from 10 to 1 MHz (for the same rf voltage $V_{rf}=500$ V), the maximum sheath thickness increases from 0.6 to 1.6 cm [see Figs. 6, 9, and 14(a)]; this can be explained as follows: When F decreases, the electron losses to the electrodes tend to be larger and must be compensated for by a larger electron multiplication in the gap; this is made possible by an increase of the sheath thickness.

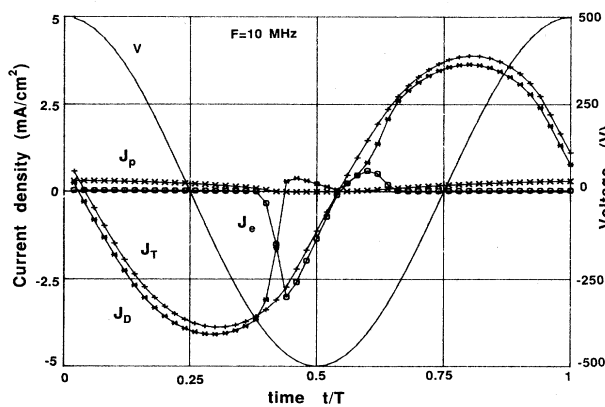


FIG. 3. Time variations of the electron (J_e , $\circ-\circ-\circ$); positive ion (J_p , $***$); displacement (J_D , $+++$); and total (J_T , $++++$) current densities on one electrode; the applied potential is also represented (V , $—$) (same conditions as Fig. 1).

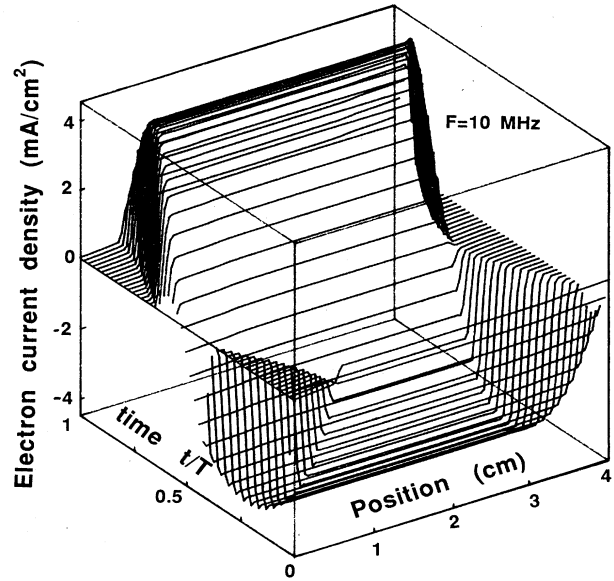


FIG. 4. Spatio-temporal variations of the electron conduction current density (same conditions as Fig. 1).

B. Electronegative gas

For $F=10$ MHz, the spatio-temporal variations of the electric field in the electropositive (Fig. 1) and electronegative (Fig. 7) gas are very similar. As can be seen in Fig. 7, ion densities in the plasma are much larger in the electronegative gas than in helium, due to the low mobility of negative ions compared with that of electrons. The low negative-ion mobility is also responsible for the smaller maximum sheath thickness in the electronegative gas (compare Figs. 1 and 7). The differences in the maximum

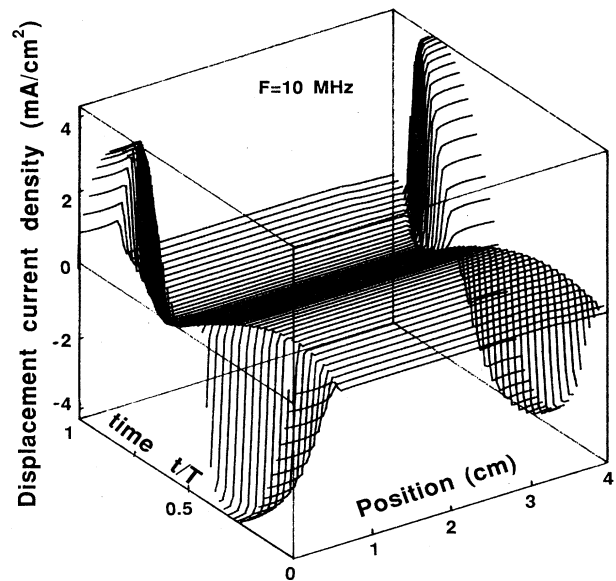


FIG. 5. Spatio-temporal variations of the displacement current density (same conditions as Fig. 1).

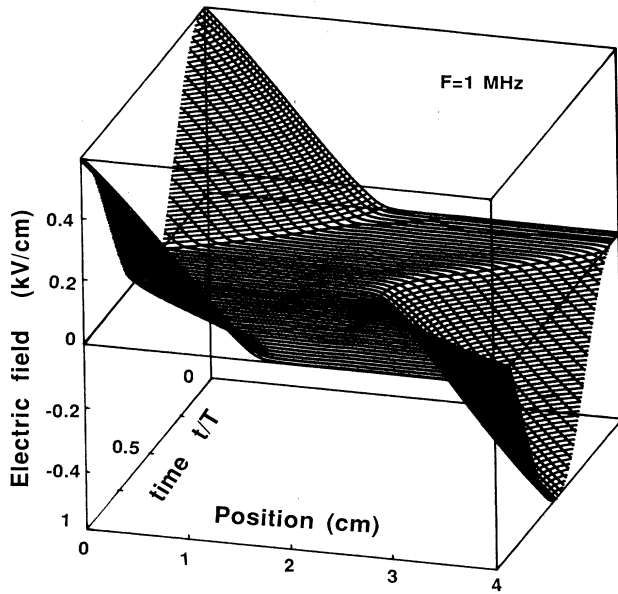


FIG. 6. Spatio-temporal variations of the electric field $F=1$ MHz, $V_{rf}=500$ V, helium).

sheath thickness in helium and in the electronegative gas are more pronounced at lower frequencies (see Figs. 6, 9, 10, and 14). The electron density in the plasma being lower in the case of the model electronegative gas (due to attachment), the electron flux to one electrode during the anodic part of a cycle tends to be smaller than in helium: A lower total electron multiplication in the gap is therefore necessary to sustain the discharge. This decrease of the electron multiplication is achieved by a sheath contraction (for the same rf voltage). The decrease in the sheath thickness when adding an electronegative gas to an electropositive gas is in agreement with experimental results.^{42,44} Although the experimentally observed sheath contraction could be also attributed to changes in electron transport coefficients (especially the ionization coefficient)

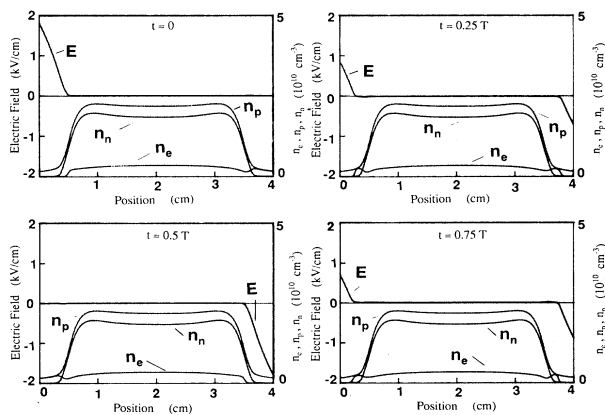


FIG. 7. Spatial variations of the electric field and charged-particle densities at four different times of a rf cycle ($f=10$ MHz, $V_{rf}=500$ V, electronegative gas).

when the electronegative gas is added,^{42,18} our results tend to prove that the only presence of negative ions induces a sheath contraction (electron transport coefficients in our model electronegative gas are the same as in helium).

The time variations of the current densities on the electrodes at 10 MHz (Fig. 8) are similar to those obtained in helium (Fig. 3). Figure 8 shows the time-averaged spatial variations of the electron, positive-ion, and negative-ion current densities. There is no significant negative-ion current to the electrode at any time of the cycle, the duration of the anodic part of the cycle being too short to allow negative ions to reach the electrodes; negative ions are maintained in the bulk plasma by the sheath oscillations. The only negative-ion loss process is therefore recombination (detachment could be important in the sheath, but at high frequencies negative ions cannot enter the sheath regions, even during the anodic part of the cycle, as mentioned above). At much lower frequencies (around 50 kHz), the negative-ion current density to the electrode becomes more significant.

The above results show that electronegative and electropositive mixtures behave similarly at high frequencies. When the frequency is decreased from 10 to 1 MHz, significant qualitative differences between electropositive and electronegative gases appear. As shown in Figs. 9(a), 10, and 14(b) the electric field presents a relative maximum at the plasma-sheath boundary, during the anodic part of the cycle. This maximum of the electric field has been observed experimentally by Gottscho *et al.*,^{6,45} in rf discharges in BCl_3 , for frequencies below the ion plasma frequency: The space-time profiles of the measured sheath fields displayed in Fig. 8 of Ref. 6 show that the electric field exhibits a maximum at the plasma-sheath boundary throughout most of the anodic half cycle, in agreement with our results. The calculated spatial variations of the charged-particle densities which are also plotted on Fig. 9(a) show that these relative field maxima are due to the formation of double layers (negative ions and positive ions) at the plasma-sheath bound-

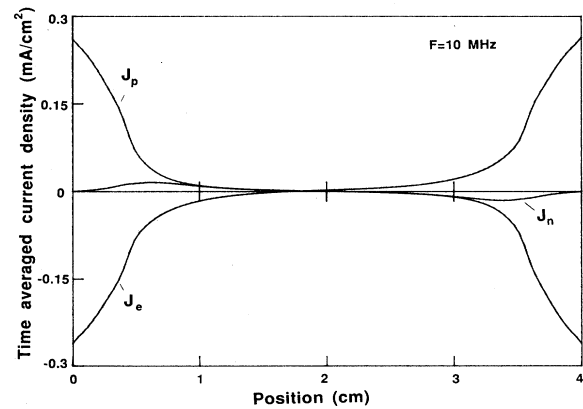


FIG. 8. Spatial variations of the time-averaged current densities (same conditions as Fig. 7).

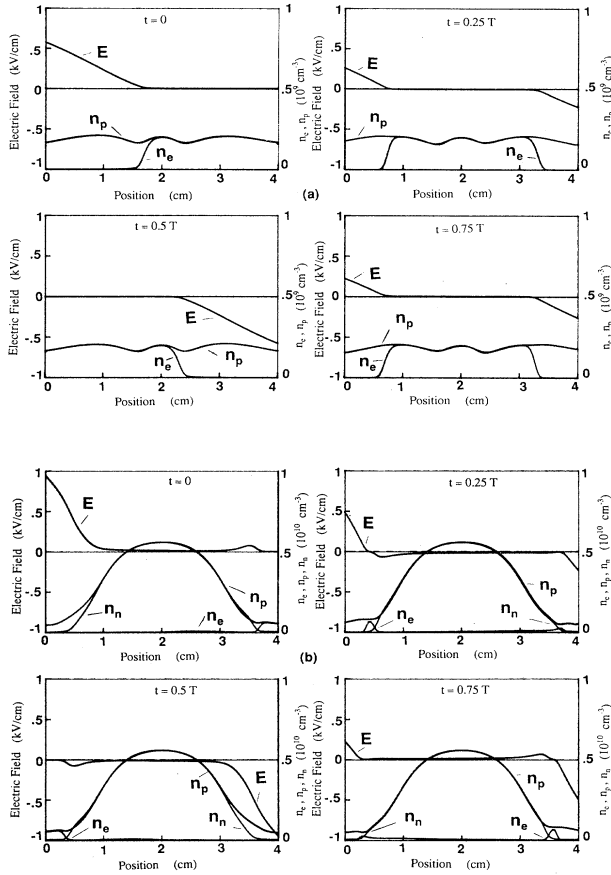


FIG. 9. (a) Spatial variations of the electric field and charged-particle densities at four different times of a rf cycle ($F=1$ MHz, $V_{rf}=500$ V, electronegative gas). (b) Spatial variations of the electric field and charged-particle densities at four different times of a rf cycle ($F=1$ MHz, $V_{rf}=500$ V, helium).

daries [let us note that these field maxima exist at 10 MHz, but with much smaller amplitudes—see Fig. 14(b)]. At 1 MHz, the ion modulation is still small compared to the electron density modulation, but due to the large ion number densities in the plasma, small density modulations can produce significant field variations. A Fourier analysis [Fig. 11(c)] of the negative-ion density shows that the negative-ion density modulation is maximum at the plasma-sheath boundary. The amplitude of the fundamental $n_n^1(x)$ is as large as the amplitude of the dc component $n_n^0(x)$ of the negative-ion density $n_n(x,t)$ at the plasma-sheath boundary and shrinks to zero in the center of the plasma (for purely rf voltages, the center of the plasma is the center of symmetry of the discharge; the odd components of the Fourier expansion must therefore be zero at that point). The large value of the fundamental $n_n^1(x)$ at the plasma-sheath boundary is due to the fact that negative ions tend to reach the electrode during the anodic part of the cycle, whereas they are repelled into the plasma by the expanding sheath during the cathodic part of the cycle. The positive-ion density modulation is similar to the negative-ion density modulation in the plasma but is smaller at the plasma

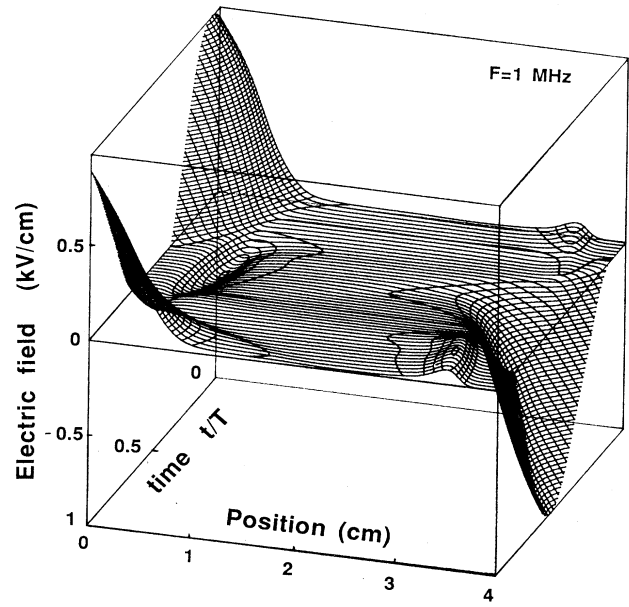


FIG. 10. Spatio-temporal variations of the electric field ($F=1$ MHz, $V_{rf}=500$ V, electronegative gas).

sheath boundary, as seen on Figure 11(b). The amplitude of the first harmonic n_k^2 is larger than the fundamental n_k^1 near the plasma center for electrons, positive ions and negative ions [Figs. 11(a), 11(b), 11(c)]; this result is in qualitative agreement with the experimental measurements of the N_2^+ concentration in a rf discharge in nitrogen⁴⁵ (see also the experimental study of rf chlorine plasmas, Ref. 46). The large modulation of the electron number density in the sheaths appears clearly on Fig. 11(a); note also the large amplitude of the first harmonic of the electron density in the plasma.

Our results show that the double-layer formation can be explained simply by a larger ion modulation at the plasma-sheath boundary, at low frequencies: detachment or non equilibrium effects (see Ref. 42) do not seem to play a fundamental role in the development of double layers at the plasma-sheath boundary. Calculations including detachment (with a detachment coefficient increasing linearly with the electric field) show that detachment tends to lessen the net charge density in the double layer, without altering the qualitative features described above.

The time variations of the current densities on the electrodes for $F=1$ MHz in helium and in the model electronegative gas exhibit features similar to those at 10 MHz; the positive-ion component of the conduction current density is, however, relatively larger than at higher frequencies, due to the larger modulation of the ion density. Figures 12(a) and 12(b) show the time variations of the electron, ion, displacement, and total current densities in the plasma center, in helium, and in the model electronegative gas at 1 MHz. In the case of helium [Fig. 12(a)], the ion current density is negligible in the plasma and the displacement current density is of the same order of magnitude as the electron current den-

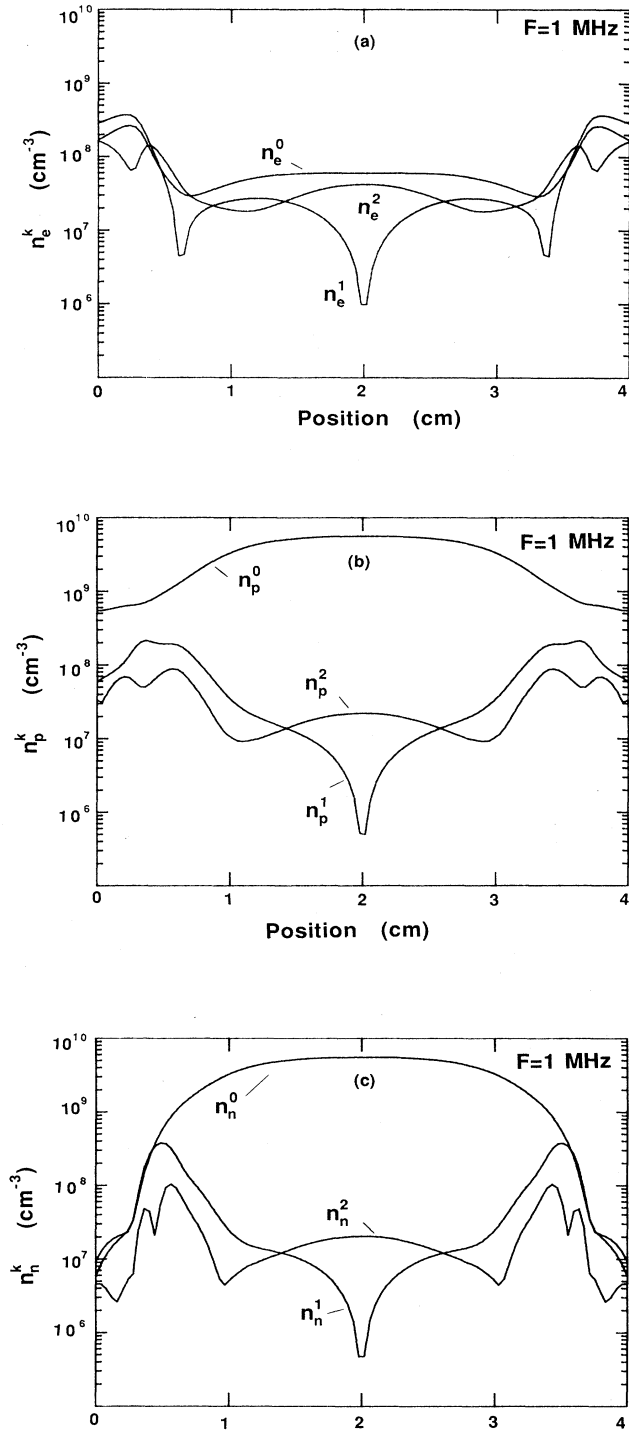


FIG. 11. (a) Spatial variations of the amplitudes of the first three terms (n_e^0 , n_e^1 , n_e^2) of the Fourier expansion of the electron number density ($F=1$ MHz, $V_{rf}=500$ V, electronegative gas). (b) Spatial variations of the amplitudes of the first three terms (n_p^0 , n_p^1 , n_p^2) of the Fourier expansion of the positive-ion number density ($F=1$ MHz, $V_{rf}=500$ V, electronegative gas). (c) Spatial variations of the amplitudes of the first three terms (n_n^0 , n_n^1 , n_n^2) of the Fourier expansion of the negative-ion number density ($F=1$ MHz, $V_{rf}=500$ V, electronegative gas).

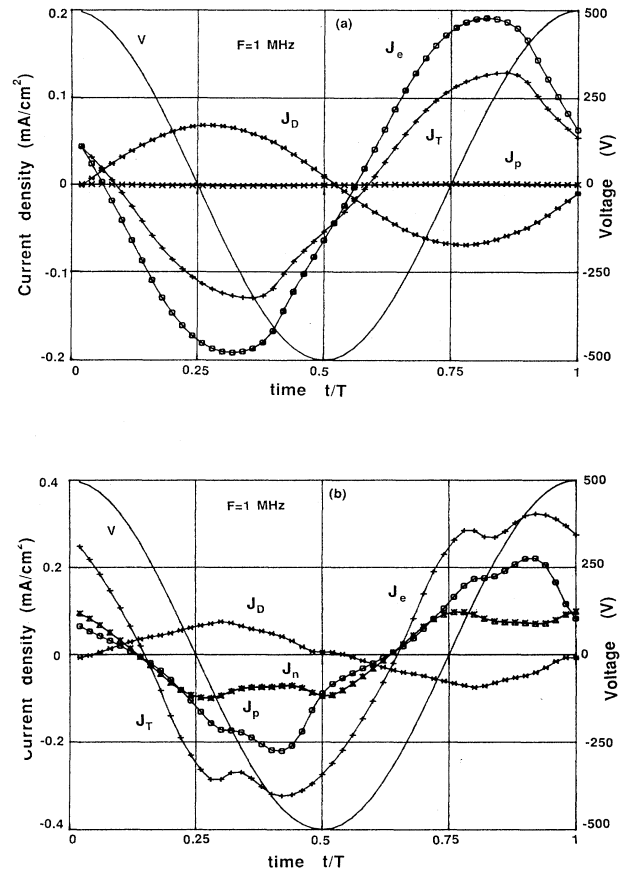


FIG. 12. (a) Time variations of the electron (J_e , $\circ\circ\circ$), ion (J_p , $\times\times\times$), displacement (J_D , $\ast\ast\ast$); and total (J_T , $+++$) current densities in the plasma center; the applied voltage is also represented (V , $—$); ($F=1$ MHz, $V_{rf}=500$ V, helium). (b) Time variations of the electron (J_e , $\circ\circ\circ$); positive ion (J_p , $\times\times\times$), negative ion (J_n , $\triangle\triangle\triangle$); displacement (J_D , $\ast\ast\ast$); and total (J_T , $+++$) current densities in the plasma center; voltage (V , $—$); ($F=1$ MHz, $V_{rf}=500$ V, electronegative gas).

sity; electron conduction current and displacement current exhibit a phase shift close to π . The time evolution of the current densities in the plasma center is more complex in the electronegative gas [Fig. 12(b)]: Positive- and negative-ion current densities are equal and are of the same order of magnitude as the displacement and electron current densities. Note the important distortion of the total current in the model electronegative gas. In agreement with experimental measurements,^{42,47} the distortion of the total current density seems to be more important at low frequencies, as can be seen in Fig. 13. The change in the current waveform with frequency compares very well with the experimental measurements (for BCl_3 plasmas) of Gottscho and Mandich shown in Fig. 7 of Ref. 47. The phase shift between voltage and current waveforms decreases when the frequency decreases: The phase shift is close to $\pi/2$ at high frequencies, whereas current and voltage are nearly in phase at low frequencies. This property of the sheath reactance is

well known,⁴⁸ the sheath being mainly capacitive at high frequencies (large displacement current, small ion density modulation), and more resistive at low frequencies (larger conduction currents, the ions being more sensitive to the time-varying field). The nonsinusoidal current waveforms displayed in Fig. 13 show that the sheath capacitances and the conduction currents through the sheaths are time varying;⁴⁹ the physical properties of the sheaths which can be deduced from our model can help in the improvement of the representation of plasma reactors by equivalent circuit models.⁵⁰

Let us note finally that the sheath thickness [Fig. 14(b)] is nearly constant in the electronegative gas, when the frequency decreases from 1 MHz to 50 kHz (for a constant rf voltage $V_{rf}=500$ V). For frequencies higher than 1 MHz, the maximum sheath thickness decreases with increasing frequency; the experimental results obtained by Gottscho⁴² in BCl_3 exhibit opposite trends. This discrepancy could be explained (see Ref. 42) by a less efficient attachment at high frequency, due to the incomplete relaxation of the electron energy distribution function (nonequilibrium effect); however, it appears from our calculations that the maximum sheath thickness at $F=10$ MHz would still be smaller than at $F=1$ MHz, even if attachment were completely neglected [see Fig. 14(a)]. The reason for this qualitative discrepancy between our results and the experimental measurements of Gottscho is therefore not clear, and may be due to some specific properties

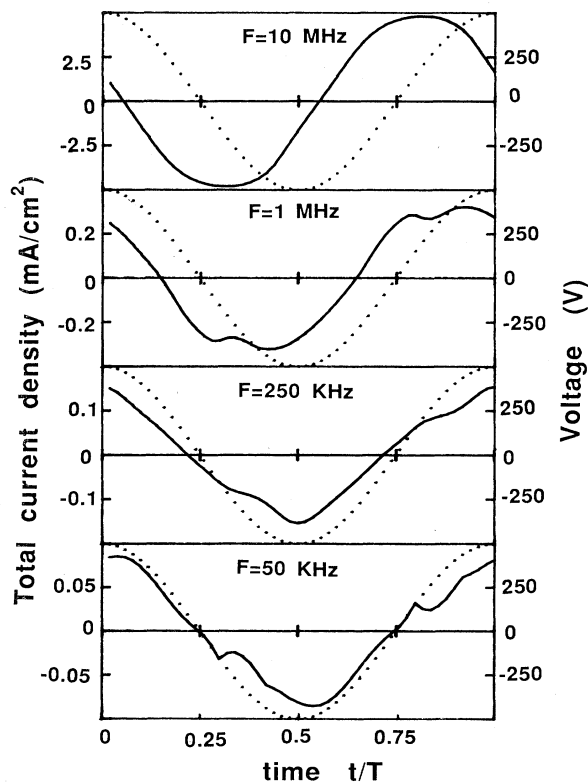


FIG. 13. Current and potential waveforms in the model electronegative gas, for different frequencies ($V_{rf}=500$ V).

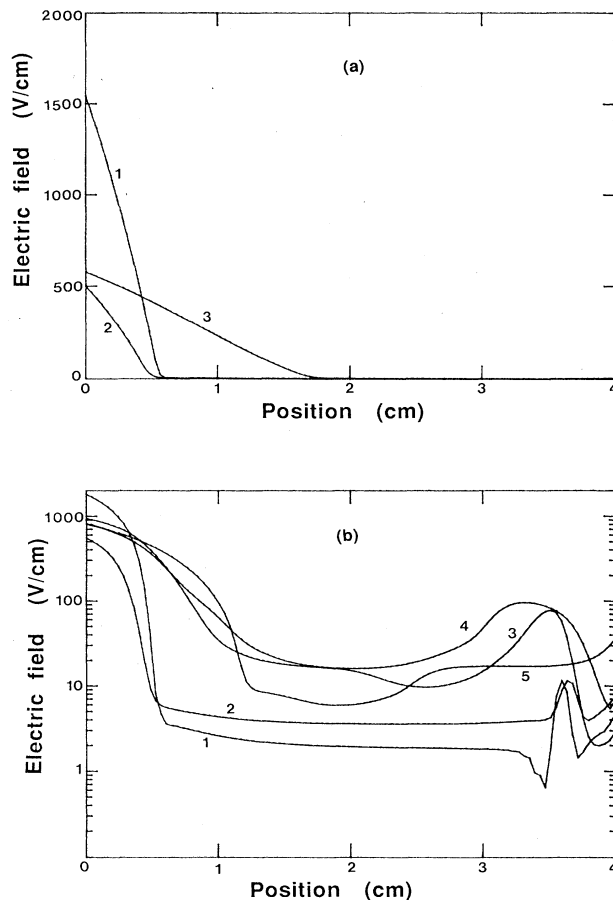


FIG. 14. (a) Spatial variations of the electric field during the cathodic part of the cycle ($t=0$) in helium for different conditions: (1) $F=10$ MHz, $V_{rf}=500$ V; (2) $F=10$ MHz, $V_{rf}=150$ V; (3) $F=1$ MHz, $V_{rf}=500$ V. (b) Spatial variations of the electric field during the cathodic part of the cycle ($t=0$) in the model electronegative gas for different conditions: (1) $F=10$ MHz, $V_{rf}=500$ V; (2) $F=10$ MHz, $V_{rf}=150$ V; (3) $F=1$ MHz, $V_{rf}=500$ V; (4) $F=250$ kHz, $V_{rf}=500$ V; (5) $F=50$ kHz, $V_{rf}=500$ V.

of BCl_3 which are not included in our model electronegative gas.

The electric field distributions displayed in Fig. 14 correspond to the cathodic part of the cycle (for the left electrode), at time $t=0$. A logarithmic scale has been used on Fig. 14(b) in order to see more clearly the field variations in the plasma and in the double layers. As mentioned above there is a small relative maximum of the electric field at the plasma-sheath boundary even at high frequencies. For $F=50$ kHz, the double layer, though not apparent at time $t=0$, on Fig. 14(b), appears at later times, during the anodic part of the cycle for the right-hand-side electrode.

IV. CONCLUSION

A self consistent model of rf glow discharges, based on a macroscopic description of the charged-particle kinetics coupled with Poisson's equation, has been presented. In

spite of its simplicity (nonlocal effects are not taken into account), this model can provide a very good picture of the physical properties of the rf discharge, in a limited range of frequency, voltage, and pressure. The efficiency of the numerical method which has been used in this work makes possible the investigation of more realistic situations involving complex molecular gases typically used in plasma processing; a detailed quantitative description of the chemical kinetics in the bulk plasma as well as in the sheaths will be useful in the control and improvement of processing reactors. On the other hand, such calculations can help in determining equivalent circuit models for plasma processing reactors.

The results are in good qualitative agreement with the most recent experimental investigations of field and charge distributions in rf discharges. The effect of frequency and negative ions on the discharge properties are summarized below.

The numerical results show that the plasma-sheath boundary oscillates in the frequency range which has been investigated (50 kHz to 10 MHz at $p=1$ torr). The sheath oscillations impart energy to the plasma electrons and increase the ionization efficiency. In the case of helium the numerical model predicts a decrease of the maximum sheath length with increasing frequency (for a constant rf voltage amplitude). The same trend is obtained in the case of the model electronegative gas above 1 MHz (at $p=1$ torr), the maximum sheath thickness being nearly constant below 1 MHz. The sheath is primarily capacitive at high frequency and more resistive at low frequency.

The presence of negative ions in the discharge leads to the formation of double layers and field maxima at the plasma-sheath boundaries, in agreement with recent experimental measurements in BCl_3 . The double-layer formation is due to a large modulation of the negative- and positive-ion density at the plasma-sheath boundary, and is more pronounced at intermediate and low frequencies (ions do not respond to the time-varying electric field at high frequencies). On the other hand, the presence of negative ions in the discharge induces a sheath contraction.

The possible effects of nonequilibrium electron transport on the above results can be studied by adding the electron energy equation to the continuity and momentum transfer equations, with adequate closure relations. The present work has demonstrated the ability of our model to predict the qualitative features of rf glow discharges. Detailed comparisons with experimental results in BCl_3 will determine to which extent the quantitative data provided by this model are reliable. Work is continuing along these lines.

ACKNOWLEDGMENTS

The author would like to thank R. A. Gottscho for sending his recent reports of his work prior to publication, L. C. Pitchford for her encouragements to pursue this work, and P. Ségur for helpful discussions concerning the numerical methods. This work has been developed, in part, in the framework of the European

Group on Gas Discharges and had been started while the author was at the Laboratoire de Physique des Décharges du Centre National de la Recherche Scientifique Gif-sur-Yvette, France. The author is with Unité Associée No. 277 du Centre National de la Recherche Scientifique at the Centre de Physique Atomique de Toulouse.

APPENDIX: IMPLICIT EXPONENTIAL SCHEME FOR THE CONTINUITY EQUATIONS

Let φ , n , W , and D be, respectively, the flux, number density, drift velocity, and diffusion coefficient of a given type of charged species; from the momentum transfer equation, we have

$$\varphi = nW - \partial_x(nD). \quad (9)$$

A standard difference approximation of the above expression would lead to numerical instabilities whenever the voltage change between mesh points is of the order or larger than the characteristic energy D/μ ($\mu = |W|/E$ is the mobility). The basic idea of the exponential scheme³⁸ is to assume that the particle flux, drift velocity, and diffusion coefficient are constant between mesh points; integration of the above equation then leads to

$$\begin{aligned} \varphi_{i+1/2} = & (1/\Delta x)[n_i D_i \exp(z_{i+1/2}) - n_{i+1} D_{i+1}] \\ & \times z_{i+1/2} / \exp(z_{i+1/2} - 1), \end{aligned} \quad (10)$$

where the $i + \frac{1}{2}$ mesh point is located midway between the major mesh points i and $i + 1$ and Δx is the distance between mesh points (a uniform mesh has been used in the calculations); $z_{i+1/2}$ is defined by

$$z_{i+1/2} = -s\mu_{i+1/2}/D_{i+1/2}(V_{i+1} - V_i).$$

V_i is the potential on mesh point i ; s is set to $+1$ for positive ions and to -1 for electrons or negative ions.

The main advantage of the difference scheme (10) is that it provides numerically stable estimates of the particle flux under all conditions; if the voltage between adjacent mesh points is large ($z_{i+1/2} \gg 1$), Eq. (10) approaches the drift flux, while it approaches the standard difference relation for the diffusion flux when the voltage between adjacent mesh points is small ($|z_{i+1/2}| \ll 1$); let us note that expression (10) is valid for positive and negative values of the parameter z so that the proposed difference scheme can deal with field reversals.

Using Eq. (10), the continuity equation is approximated by the following difference scheme:

$$\begin{aligned} [(n_{i+1})^{k+1} - (n_i)^{k+1}]/\Delta t + [(\varphi_{i+1/2})^{k+1} \\ - (\varphi_{i-1/2})^{k+1}]/\Delta x = (S_i)^k, \end{aligned} \quad (11)$$

Δt being the time step and S_i the source term at mesh point i ; superscripts k and $k + 1$ refer to time t^k and t^{k+1} , respectively ($t^{k+1} = t^k + \Delta t$). Electric field, potential, transport coefficients, and source terms involved in Eq. (11) are calculated at time t^k , whereas densities are taken at time t^{k+1} in $(\varphi_{i+1/2})^{k+1}$ and $(\varphi_{i-1/2})^{k+1}$; Eq.

(11) is therefore a tridiagonal system in $(n_{i-i})^{k+1}$, $(n_i)^{k+1}$, $(n_{i+1})^{k+1}$ which can be solved with a standard Gaussian elimination method. Let us note that internal iterations could be used in order to solve Poisson and

continuity equations together instead of alternatively; this iterative procedure was not found necessary due to the small time step used in the calculations (a few 10^{-3} of the cycle duration).

- ¹R. A. Gottscho and T. A. Miller, *Pure Appl. Chem.* **56**, 189 (1984).
- ²C. A. Moore, G. P. Davis, and R. A. Gottscho, *Phys. Rev. Lett.* **52**, 538 (1984).
- ³D. K. Doughty, S. Salih, and J. E. Lawler, *Phys. Lett.* **103A**, 41 (1984).
- ⁴B. N. Ganguly and A. Garscadden, *Phys. Rev. A* **32**, 2544 (1985).
- ⁵J. Derouard and N. Sadeghi, *Opt. Commun.* **57**, 239 (1986).
- ⁶R. A. Gottscho and C. E. Gaebe, *IEEE Trans. Plasma Sci.* **PS-14**, 92 (1986).
- ⁷M. J. Kushner, *J. Appl. Phys.* **54**, 4958 (1983).
- ⁸M. J. Kushner, *J. Appl. Phys.* **53**, 1942 (1982).
- ⁹H. Chatham and A. Gallagher, *J. Appl. Phys.* **58**, 159 (1985).
- ¹⁰D. B. Graves and K. F. Jensen, *IEEE Trans. Plasma Sci.* **PS-14**, 78 (1986).
- ¹¹M. S. Barnes, T. J. Cotler, and M. E. Elta, *J. Appl. Phys.* **61**, 81 (1987).
- ¹²A. D. Richards, B. E. Thompson, and H. H. Sawin, *Appl. Phys. Lett.* **50**, 492 (1987).
- ¹³J. P. Boeuf and E. Marode, *J. Phys. D* **15**, 2169 (1982); L. E. Kline, *J. Appl. Phys.* **58**, 3715 (1985); T. J. Moratz, L. C. Pitchford, and J. N. Bardsley, *ibid.* **61**, 2146 (1987).
- ¹⁴P. Ségur, M. Yousfi, J. P. Boeuf, E. Marode, A. J. Davies, and J. G. Evans, in *Electrical Breakdown and Discharges in Gases*, Vol. 89a of *NATO Advanced Study Institute, Series B: Physics*, edited by E. E. Kunhardt and H. L. Luessen, (Plenum, New York, 1983), p. 331.
- ¹⁵N. Sato and H. Tagashira, *J. Phys. D* **18**, 2451 (1985).
- ¹⁶W. P. Allis, G. Fournier, and D. Pigache, *J. Phys. (Paris)* **38**, 915 (1977).
- ¹⁷W. H. Long, Jr., Northrop Research and Technology Center, Tech. Rep. No. AFAPL-TR 79-2038, 1979 (unpublished).
- ¹⁸G. L. Duke, Aero Propulsion Laboratory, Tech. Rep. No. AFWAL-TR-84 2099 (1985) (unpublished).
- ¹⁹Von Engel, *Ionized Gases* (Oxford University Press, New York, 1965).
- ²⁰A. L. Ward, *Phys. Rev.* **112**, 1852 (1958); *J. Appl. Phys.* **33**, 2789 (1962).
- ²¹J. J. Lowke and D. K. Davies, *J. Appl. Phys.* **48**, 4991 (1977).
- ²²A. J. Davies and J. G. Evans, *J. Phys. D* **13**, L161 (1980).
- ²³J. H. Ingold, in *Gaseous Electronics*, edited by M. N. Hirsh and H. J. Oskam (Academic, New York, 1978), Vol. 1, p. 19.
- ²⁴J. P. Boeuf, A. J. Davies, J. G. Evans, E. Marode, and P. Ségur, in *Proceedings of the Seventh International Conference on Gas Discharges and their Applications, London* (Peter Peregrinus, London, 1982).
- ²⁵P. Bayle, J. Vacquie, and M. Bayle, *Phys. Rev. A* **34**, 360 (1986).
- ²⁶J. M. S. Schofield, in *Proceedings of the International Conference on Phenomena in Ionized Gases XII*, edited by J. G. A. Holscher and D. R. Schram (North-Holland, Amsterdam, 1975), Part I, p. 73.
- ²⁷Tran Ngoc An, E. Marode, and P. C. Johnson, *J. Phys. D* **10**, 2317 (1977).
- ²⁸P. J. Roache, *Computational Fluid Dynamics*, (Hermosa, Albuquerque, New Mexico, 1974).
- ²⁹K. Kumar, H. R. Skullerud, and R. E. Robson, *J. Aust. Phys.* **33**, 343 (1980).
- ³⁰R. Winkler, H. Deutsch, J. Wilhelm, and Ch. Wilke, *Beitr. Plasmaphys.* **24**, 285 (1984); **24**, 303 (1984).
- ³¹R. Winkler, J. Wilhelm, and A. Hess, *Ann. Phys., Leipzig* **42**, 537 (1985).
- ³²L. S. Frost and A. V. Phelps, *Phys. Rev.* **127**, 1621 (1962).
- ³³L. E. Kline, *IEEE Trans. Plasma Sci.* **PS-14**, 145 (1986).
- ³⁴G. L. Rogoff, J. M. Kramer, and R. B. Piejak, *IEEE Trans. Plasma Sci.* **PS-14**, 103 (1986).
- ³⁵S. Selberherr, *Analysis and Simulation of Semiconductor Devices* (Springer, Vienna, 1984).
- ³⁶S. Selberherr and C. A. Ringhofer, *IEEE Trans. Comput.-Aided Design CAD-3*, 52 (1984).
- ³⁷C. M. Snowden, *Rep. Prog. Phys.* **45**, 223 (1985).
- ³⁸D. L. Sharfetter and H. K. Gummel, *IEEE Trans. Electron. Devices ED-16*, 64 (1969); see also H. K. Gummel, *ibid.* **ED-30**, 1097 (1964), and A. De Mari, *Solid State Electron.* **11**, 33 (1968).
- ³⁹M. S. Mock, *Solid State Electron.* **24**, 959 (1981).
- ⁴⁰B. S. Polsky and J. S. Rimshans, *Solid State Electron.* **29**, 321 (1986).
- ⁴¹S. V. Patankar, *Numerical Heat Transfer and Fluid Flow* (Hemisphere, 1980).
- ⁴²R. A. Gottscho, *Phys. Rev. A* **36**, 2233 (1987).
- ⁴³V. A. Godyak, *Fiz. Plazmy* **2**, 141 (1976) [*Sov. J. Plasma Phys.* **2**, 78 (1976)].
- ⁴⁴K. G. Emeleus and G. A. Wolsey, *Discharges in Electronegative gases* (Barnes and Noble, New York, 1970).
- ⁴⁵R. A. Gottscho, R. H. Burton, D. L. Flamm, V. M. Donnelly, and G. P. Davis, *J. Appl. Phys.* **55**, 2707 (1984).
- ⁴⁶D. L. Flamm and V. M. Donnelly, *J. Appl. Phys.* **59**, 1052 (1986).
- ⁴⁷R. A. Gottscho and M. L. Mandlich, *J. Vac. Sci. Technol. A* **3**, 617 (1985).
- ⁴⁸B. Chapman, *Glow Discharge Processes*, (Wiley, New York, 1980).
- ⁴⁹A. Metzke, D. W. Ernie, and H. J. Oskam, *J. Appl. Phys.* **60**, 3081 (1986).
- ⁵⁰A. J. Van Roosemalen, W. G. M. van den Hoek, and H. Kalter, *J. Appl. Phys.* **58**, 653 (1985); K. Köhler, D. E. Horne, and J. W. Coburn, *J. Appl. Phys.* **58**, 3350 (1985).